

Glucose-Responsive Hybrid Nanoassemblies in Aqueous Solutions: Ordered Phenylboronic Acid within Intermixed Poly(4-hydroxystyrene)-*block*-poly(ethylene oxide) Block Copolymer

Alicja Matuszewska,^{†,‡} Mariusz Uchman,^{*,†} Agnieszka Adamczyk-Woźniak,[‡] Andrzej Sporzyński,[‡] Stergios Pispas,[§] Lubomír Kováčik,^{||} and Miroslav Štěpánek[†]

[†]Department of Physical and Macromolecular Chemistry Faculty of Science, Charles University in Prague, Hlavova 2030, 128 40 Prague 2, Czech Republic

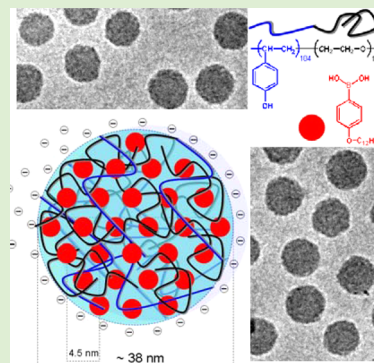
[‡]Department of Physical Chemistry, Faculty of Chemistry, Warsaw University of Technology, Noakowskiego 3, 00664 Warsaw, Poland

[§]Theoretical & Physical Chemistry Institute, National Hellenic Research Foundation, 48 Vassileos Constantinou Avenue, 11635 Athens, Greece

^{||}Institute of Cellular Biology and Pathology, First Faculty of Medicine, Charles University in Prague, Albertov 4, 128 01 Prague 2, Czech Republic

Supporting Information

ABSTRACT: Coassembly behavior of the double hydrophilic block copolymer poly(4-hydroxystyrene)-*block*-poly(ethylene oxide) (PHOS-PEO) with three amphiphilic phenylboronic acids (PBA) differing in hydrophobicity, 4-dodecyloxyphenylboronic acid (C12), 4-octyloxyphenylboronic acid (C8), and 4-isobutoxyphenylboronic acid (*i*-Bu) was studied in alkaline aqueous solutions and in mixtures of NaOH_{aq}/THF by spin-echo ¹H NMR spectroscopy, dynamic and electrophoretic light scattering, and SAXS. The study reveals that only the coassembly of C12 with PHOS-PEO provides spherical nanoparticles with intermixed PHOS and PEO blocks, containing densely packed C12 micelles. NMR measurements have shown that spatial proximity of PHOS-PEO and C12 leads to the formation of ester bonds between -OH of PHOS block and hydroxyl groups of -B(OH)₂. Due to the presence of PBA moieties, the release of compounds with 1,2- or 1,3-dihydroxy groups loaded in the coassembled PHOS-PEO/PBA nanoparticles by covalent binding to PBA can be triggered by addition of a surplus of glucose that bind to PBA competitively. The latter feature has been confirmed by fluorescence measurements using Alizarin Red as a model compound. Nanoparticles were proved to exhibit swelling in response to glucose as detected by light scattering.



INTRODUCTION

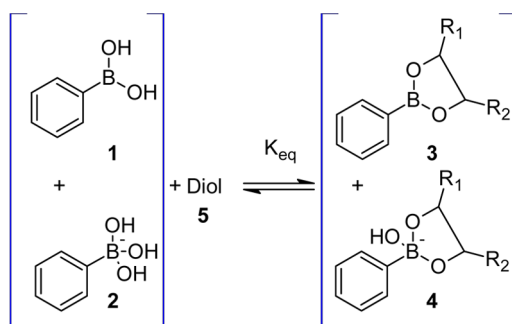
Diabetes is a group of metabolic diseases characterized by high glucose levels in blood caused by inadequate insulin secretion or insulin action. The World Health Organization (WHO) projects that 347 million people have diabetes, and this number is expected to reach 440 million in 20 years.¹ Moreover, it is predicted to become the seventh major cause of death in the world by the year 2030. For type 1 diabetes, caused by defects in insulin production, blood sugar range has been controlled so far by insulin injections; therefore, the development of noninjectable treatment has been under investigation for decades. An insulin-loaded polymer system for controlled polypeptide release is one of the approaches which has been widely investigated.² Most systems for triggered release of drugs are based on block copolymer micelles.^{3–6}

Phenylboronic acids (PBA) are an important group of chemical receptors⁷ due to reversible, covalent binding of *cis*-1,2- and 1,3-diols,^{8–10} high stability^{11,12} and low toxicity. There

have been reported just few water-soluble, cosolvent-free systems based on PBA¹³ that are able to recognize biologically important polyols like glucose.¹⁴ PBA exists in two forms which are in equilibrium in water. The tetragonal PBA can form glucose-boronate complexes and therefore shift the equilibrium toward a more hydrophilic form. Phenylboronic acids exist in two forms neutral-trigonal (1, 3) and anionic-tetragonal form (2, 4), which are in equilibrium in water (Scheme 1).

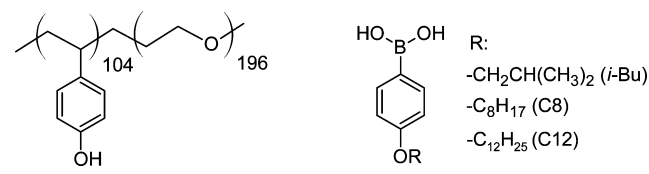
A complex system combining polymer as a matrix and phenylboronic acid as a sensor seems to be an effective solution allowing for detection of carbohydrates, as well as for controlled drug release. As a result, a series of research works have been conducted to obtain glucose-sensitive gels,^{16,17} microgels,^{18–21} polymers,²² or glycopolymers.^{23–25} One of the systems which have been under investigation is polymer gel, swelling of which

Received: May 13, 2015

Scheme 1. Equilibrium of Phenylboronic Acids and Their Esters¹⁵

(and consequently the release of insulin loaded in it) can be controlled by the concentration of glucose. This on-off insulin release gel based on poly(*N*-isopropylacrylamide) (PNIPAAm) derivatized with a definite fraction of a phenylboronic acid group and a small amount of *N,N'*-methylenebisacrylamide (NMBA) as a cross-linker may be used in self-regulated drug-releasing systems. Poly(*N*-isopropylacrylamide)-based phenylboronic acid (PNIPAM-based PBA) functionalized microgels were designed to form nanoparticles which swell in response to increase in the glucose concentration.¹⁸ Linear trends have been observed in light scattering intensity and hydrodynamic diameter for binding glucose by microgel in specific range of sugar (0–0.2 mg/mL). Temperature, 1,2- and 1,3-diols-, and pH-sensitive block copolymers containing boronic acid were synthesized by reversible addition-fragmentation chain transfer (RAFT) polymerization.²² Dissociation of poly(3-acrylamidophenylboronic acid)-*block*-poly(*N*-isopropylacrylamide) (PAPBA-*b*-PNIPAM) aggregates to unimers occurred upon addition of NaOH at pH 11 or glucose at pH 8.7. Low toxicity polymeric vehicles of poly(ethylene glycol)-*block*-poly[(2-phenylboronic esters-1,3-dioxane-5-ethyl) methyl acrylate] (MPEG5000-*b*-PBDEMA) were obtained via atom transfer radical polymerization (ATRP).²⁶ MPEG5000-*b*-PBDEMA can aggregate into a spherical core-shell structure. Insulin-loaded MPEG5000-*b*-PBDEMA nanoparticles responded to glucose concentration at physiological conditions (pH = 7.4 and 37 °C). Amphiphilic glycopolymer poly(acrylic acid-*co*-acrylamidophenylboronic acid)-*block*-poly(2-acryloxyethyl galactose)-*block*-poly(acrylic acid-*co*-acrylamidophenylboronic acid) ((PAA-*co*-PAAPBA)-*b*-2PAEG) copolymer formed pH- and glucose-responsive nanoparticles. The nanoparticles were stable at pH 5.0, 7.0, and 9.0 exhibiting zeta-potential of ca. –25 mV, but aggregated and precipitated at pH 1.0 and 3.0. It was proved that glucose-responsiveness of the system and insulin release are pH dependent.²³ All mentioned systems have been designed as polymers containing boronic acid moieties.

Here we report on self-assembled nanoparticles formed in alkaline aqueous solutions by diblock copolymer poly(4-hydroxystyrene)-*block*-poly(ethylene oxide) (PHOS-PEO) with amphiphilic phenylboronic acids (PBA) (see Scheme 2). We found recently (ref 28) that solution behavior of PHOS-PEO does not resemble that of a typical diblock copolymer in selective solvent. PHOS (also referred to as poly(4-vinylphenol)) is an extremely weak polyacid with the p*K* of ca. 10 and is water-soluble in strongly alkaline aqueous solutions.²⁹ Therefore, one could expect that PHOS-PEO will behave as a double hydrophilic diblock copolymer in water at high pH and as an amphiphilic one at lower pHs, however, PHOS-PEO is

Scheme 2. Chemical Structures of Diblock Copolymer (PHOS₁₀₄-PEO₁₉₆) (Subscripts Denote Degree of Polymerization) and Phenyl Boronic Acids Used in This Study

not directly soluble even in sodium hydroxide aqueous solutions at pH 12. The reason for this behavior is kinetic: even PHOS homopolymer dissolves very slowly in alkaline aqueous solutions.³⁰ In the case of PHOS-PEO diblock, the dissolution is further slowed down, which can be explained by the formation of hydrogen bonds between PHOS and PEO.³¹ Therefore, cosolvents like THF are needed to dissolve PHOS-PEO in aqueous media. The resulting dispersions contain aggregates cross-linked by hydrogen bonds between PHOS and PEO blocks and stabilized by the negatively charged O^- groups on the surface of the aggregates. Well-defined compact spherical nanoparticles with intermixed PHOS and PEO blocks can be prepared by the transfer of the aggregates from dispersions in THF/aq. NaOH mixtures to aqueous NaOH. In this study, we use the capability of PHOS to form dynamic covalent bonds with phenylboronic acids and to incorporate PBA into coassembled nanoparticles. To the best of our knowledge, no similar approach has been proposed before. This method allows for easy nanoparticles preparation and precisely controlling inner structure of nanoparticles and their delivery profile with no need of advanced synthesis of a series of polymer. Three PBAs differing in hydrophobicity, 4-dodecyloxyphenylboronic acid (C12), 4-octyloxyphenylboronic acid (C8), and 4-isobutoxyphenylboronic acid (*i*-Bu), were used in order to tune and control the structure and properties of coassembled nanoparticles. The responsiveness of the systems to glucose was studied by fluorescence measurements using Alizarin Red as a model compound loaded in the nanoparticles as well as by light scattering. We show that introduction of PBA into PHOS-PEO nanocarrier leads to the formation of unique glucose responsive nanostructures. Special attention was paid to the interaction of PBA with a 4-alkyloxy chain and PHOS-PEO in alkaline aqueous solutions.

EXPERIMENTAL SECTION

Materials. Copolymer Sample. Poly(4-hydroxystyrene)-*block*-poly(ethylene oxide) (PHOS₁₀₄-PEO₁₉₆) copolymer ($M_w = 21.1$ kg/mol, $M_w/M_n = 1.13$, $w_{PEO} = 0.41$) was prepared by hydrolysis of poly(*tert*-butoxystyrene)-*block*-poly(ethylene oxide) precursor synthesized by sequential anionic polymerization. Details are provided in ref 27.

Alizarin (Acros Organics), glucose (>99%, Sigma-Aldrich), D₂O (99.8 atom %D, ARMER Chemicals), and NaDO (30% in D₂O 99.3% atom %D, Chemotrade) were used as received.

Phenylboronic Acid Compounds. 4-Isobutoxyphenylboronic acid (*i*-Bu) was obtained from Aldrich. 4-Octyloxyphenylboronic acid (C8) was synthesized as described in ref 32. 4-Dodecylphenylboronic acid was synthesized in similar way in short, 8.17 g (32.8 mmol) of *n*-dodecyl bromide was added to the mixture of 11.35 g (65.6 mmol) of 4-bromophenol, 0.42 g (1.3 mmol) of TBAB, and 2.62 g (65.6 mmol) of NaOH in 50 mL of water. The mixture was refluxed with stirring for 10 h. After cooling, the solid was separated, washed with 1 M NaOH and several times with water to obtain neutral pH, and finally dried on

air. The product containing unreacted dodecyl bromide was heated under vacuum to obtain 2.88 g (8.44 mmol, 25.7%) of 1-bromo-4-dodecyloxybenzene, which was used without further purification.

4-Dodecyloxyphenylboronic Acid (C12). The reaction was carried out under argon atmosphere. The mixture of diethyl ether (50 mL) and THF (10 mL) was placed in a three-necked round-bottomed flask, equipped with a CO₂/acetone bath and magnetic stirrer and was cooled down to -65 °C. *n*-Butyllithium (2.5 M in hexane, 3.70 mL, 9.28 mmol) was slowly added to the stirred solvent. 1-Bromo-4-dodecyloxybenzene (2.88 g, 8.44 mol) in 20 mL of diethyl ether was dropped-in for 10 min, while keeping the temperature below -65 °C. The obtained white slurry was stirred at ca. -70 °C for 1 h. Trimethyl borate (1.03 mL, 9.24 mmol) was dropped-in while keeping the temperature below -65 °C. The stirring was continued for 1 h at this temperature. After that time the CO₂/acetone bath was removed and 3 M HCl was quickly added during intense stirring to obtain acidic pH. The temperature rose to about 0 °C. The resulting phases were separated and the aqueous phase was extracted twice with diethyl ether (30 mL). The organic phases were combined and about 3/4 of the volume of the solvent removed under reduced pressure. Water (50 mL) was added to the remaining liquid and evaporation was continued for an additional half an hour. After that time a white solid was filtered off, washed with water and hexane, and dried on air to obtain 1.69 g (5.52 mmol, 65.7% yield) of 4-dodecyloxyphenylboronic acid. ¹H NMR (500 MHz, acetone-*d*₆) ppm: 7.77 (d, 2H), 6.85 (d, 2H), 3.96 (t, 2H), 1.75–1.23 (multiplets, 20H), 0.83 (t, 3H). ¹¹B NMR (160 MHz, acetone-*d*₆): 29.4 ppm.

Preparation of PHOS–PEO/PBA Nanoparticles in Alkaline Aqueous Solutions. Mixture of tetrahydrofuran and aqueous 10 mM sodium hydroxide (THF/aq. NaOH, 0.4:0.6, v/v) was used as the initial solvent for PHOS–PEO/PBA. An amount of 1.5 mL of THF/aq. NaOH solution containing 10 mg of PHOS–PEO and 2.45 × 10⁻⁵ mol of corresponding PBA was added dropwise to 8.5 mL of 10 mM aqueous NaOH so that the final concentrations of PHOS–PEO and PBA in the solution were 1 mg/mL and 2.45 × 10⁻³ M, respectively. The solution was then dialyzed against 10 mM aqueous NaOH (or 10 mM aqueous NaOD in D₂O for ¹H NMR and diffusion measurements) to remove THF. Following dialysis were carried out against H₂O or D₂O in order to lower pH or pD of the samples.

Methods. p*K*_a Determination. Saturated solution of 4-isobutoxyphenylboronic acid (concentration about 1.0 × 10⁻⁴ M) was dissolved in Hydrion 7.4 phosphate buffer. The pH of the solution was adjusted with sodium hydroxide. The pH measurements were performed with Schott Lab 850 pH meter. Spectrophotometric measurements for the determination of the acid dissociation constants were carried out with PerkinElmer Lambda 25 spectrophotometer. Solutions having the proper pH were placed in quartz cuvettes, and UV–vis absorption scans were performed. The spectra were analyzed by calculation of the spectral difference between the acid spectra and the spectra obtained at other pH. The wavelengths of maximum positive and negative deviations were determined graphically, and the absolute values of the absorbance difference at this wavelengths were summed. The total absorbance difference was then plotted vs pH, and the data was fit to the Henderson–Hasselbalch equation³³ to obtain the p*K*_a value.

Surface Tension Measurement. Surface tension of PBA 100 mM NaOH aqueous solutions was measured by means of the pendant drop method using a DataPhysics OCA-15 Plus, video based measurement instrument for static and dynamic contact angle (DataPhysics Instrument GmbH, Fildesstadt, Germany).

Light Scattering (LS). Light scattering measurements were performed on ALV setup (Langen, Germany) equipped with a 22 mW He–Ne laser operating at the wavelength λ = 632.8 nm, an ALV CGS/8F goniometer, an ALV High QE APD detector, and an ALV 5000/EPP multibit, multitaup autocorrelator. All samples were measured at 25 °C with the scattering angles, θ, ranging from 30° to 150°. Detail on LS data evaluation are given in the [Supporting Information](#).

¹H NMR Spectroscopy. NMR spectra were recorded on a Varian 300 spectrometer at 25 °C. For PHOS–PEO/PBA solutions in D₂O

and 10 mM NaOD in D₂O, solvent residual signal at 4.79 ppm was used as a reference. Solutions in THF-*d*₈ and mixtures of THF-*d*₈ with 10 mM NaOD in D₂O were referenced to THF-*d*₈ residual signal at 3.58 ppm. ¹¹B NMR spectra were recorded on a Varian Unity Plus 200 operating at 64 MHz at 25 °C, and chemical shifts were determined using inserts with BF₃·Et₂O in benzene (δ = 0.0 ppm).

Measurements of translational diffusion coefficients (spin–echo) were performed on Bruker Avance III 600 MHz spectrometer at 25 °C and nanoparticles concentration 1 g L⁻¹ with the double stimulated echo experiment with bipolar pulse field gradients described by Jerschow et al.³⁴ The pulse sequence has been optimized to suppress flow and convection artifacts as well as eddy current effects. The use of bipolar gradients removes possible modulation of the intensity decay curves by chemical exchange occurring between the sites with different chemical shifts.³⁵ The gradients were 1 ms long with 16 different linearly spaced amplitudes spanning the range 0–60 G cm⁻¹, and the diffusion time was 1 s. The calibration was done using a standard sample of 1% H₂O in D₂O (doped with GdCl₃), for which the value of the HDO diffusion coefficient at 25 °C is 1.9 × 10⁻⁹ m² s⁻¹.³⁶ All data processing and fitting of the diffusion coefficients has been done using the spectrometer software (Topspin 2.1, Bruker).

Small-Angle X-ray Scattering (SAXS). SAXS experiments were carried out on the P12 BioSAXS beamline at the PETRA III storage ring of the Deutsche ElektronenSynchrotron (DESY, Hamburg, Germany) at 20 °C. The beamline was equipped with a Pilatus 2 M detector and synchrotron radiation with a wavelength of λ = 0.1 nm. The sample–detector distance was 3 m, allowing to cover the *q*-range interval from 0.11 to 4.4 nm⁻¹. The *q*-range was calibrated using the diffraction patterns of silver behenate. The experimental data were normalized to the incident beam intensity and corrected for nonhomogeneous detector response, and the background scattering of the solvent was subtracted. The solvent scattering was measured before and after the sample scattering to control for possible sample holder contamination. Eight consecutive frames comprising the measurement of the solvent, sample, and solvent were performed. No measurable radiation damage was detected by the comparison of eight successive time frames with 15 s exposures. The final scattering curve was obtained using the PRIMUS program by averaging the scattering data collected from the different frames. The automatic sample changer for sample volume 15 mL and filling cycle of 20 s was used.

Electrophoretic Light Scattering. Zeta-potential (ζ-potential) was measured with a Nano-ZS zetasizer (Malvern Instruments, U.K.). ζ-Potential values were calculated as average of five subsequent measurements (each consisted of 15–100 runs) from electrophoretic mobilities using the Henry equation in the Smoluchowski approximation, μ = εζ/η, where μ is the electrophoretic mobility and ε is the dielectric constant of the solvent.

Transmission Cryo-Electron Microscopy (Cryo-TEM). Cryo-TEM was used to visualize the morphology of the objects in solution. This technique provides direct imaging of the hydrated sample without perturbing the nanoparticles. The samples for cryo-TEM were prepared as described earlier.³⁷ A volume of 3 μL of the sample solution was applied to an electron microscopy grid with carbon-covered polymer supporting film (lacey-carbon grids LC200-Cu/C, Electron Microscopy Sciences), glow discharged for 40 s with 5 mA current. Most of the sample was removed by blotting (Whatman no. 1 filter paper) for ~1 s, and the grid was immediately plunged into liquid ethane held at -183 °C. The sample was then transferred without rewarming into a Tecnai Sphera G20 electron microscope (FEI, Hillsboro, OR) using a Gatan 626 cryo-specimen holder (Gatan Inc., Pleasanton, CA). Images were recorded at 120 kV accelerating voltage and microscope magnifications ranging from 5000× to 14 500× using a Gatan UltraScan 1000 slow scan CCD camera (giving a final pixel size from 2 to 0.7 nm) and the low-dose mode with the electron dose not exceeding 1500 electrons/nm². The applied underfocus typically ranged between 1.5 and 2.7 μm. The applied blotting conditions resulted in the specimen thickness varying between 100 and ca. 300 nm.

Fluorescence Spectroscopy. Steady-state fluorescence measurements were performed in 1 cm quartz cuvettes using a FluoroLog 3-22 spectrometer (Horiba–Jobin Yvon, France) equipped with excitation and emission double monochromators and a 450 W xenon lamp as a light source and Alizarin S as a fluorescent probe. The final concentration of Alizarin Red S (ARS) in the aqueous solution of PHOS–PEO (1 mg mL^{-1})/PBA(2.5 mM) nanoparticles was 1×10^{-4} M. After mixing of ARS and nanoparticles, the solution was left for 24 h for equilibration (it was checked that the fluorescence emission intensity of the samples did not change on the time scale of hours). After the emission spectrum measurement for the equilibrated sample, $100 \mu\text{L}$ of the glucose stock solution 11.1 mM was added to the solution and the emission spectra were measured again immediately and in 1, 2, 3, and 6 h after the glucose addition.

Potentiometry. pH measurements were performed with a Radiometer PHM 93 reference pH meter equipped with PHC 3006 combined glass microelectrode.

RESULTS AND DISCUSSION

Association Behavior of PBA in 100 mM NaOH Aqueous Solution. The previous study on surfactant-like

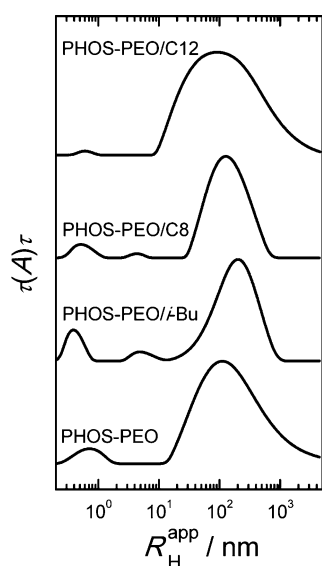


Figure 1. DLS CONTIN distribution of apparent hydrodynamic radii at the scattering angle, $\theta = 90^\circ$ of 40% THF PHOS–PEO (1), PHOS–PEO/*i*-Bu (2), PHOS–PEO/C8 (3), and PHOS–PEO/C12 (4).

PBAs solution behavior revealed that PBA undergoes aggregation in aqueous solution into variety of nanostructures like micelles, vesicles, and more complex structures.^{14,38} Our results confirm that observation, however, only for PBA C8. The micellization of alkyl phenylboronic acids derivatives strongly depends on its solubility, for example, *N*-alkyl derivatives of pyridine-3-boronic acid, which is known as one of the least basic among aryl boronic acids, with $pK_a = 4.3$ is well soluble in water at concentrations providing micelle or vesicle formation, whereas pyridine-4-boronic acid derivatives are sparingly water-soluble.¹⁴ In the case of 2-dodecylpyridine-5-boronic acid (SDDPB) and 2-oxidodecylpyridine-5-boronic acid (SODDPB) one additional oxygen atom is decreasing the critical micelle concentration at pH 13 by 1 order of magnitude.³⁸ It is why at first we determined the pK_a value of PBA *i*-Bu by the spectrophotometric method in three independent experiments giving the value of $9.1 (\pm 0.1)$ which places it among the weakest acids within the phenylboronic

acids family.³⁹ The obtained value is in good agreement with those reported for analogous compounds such as 4-methoxyphenylboronic acid as well as 4-methylphenylboronic acid (9.3)³⁹ Due to very low solubility of PBA C8 as well as PBA C12 in the applied buffer, it was impossible to determine their pK_a values but they are expected to be very close to the pK_a of the analog PBA *i*-Bu.

The surface tension, γ , measurement was performed for saturated solutions of all PBAs in 100 mM NaOH at pH 12, however only PBA C8 decreases surface tension efficiently. The direct proof that PBA C8 can be included in a broader family of surfactants is shown in Figure S1. The curve exhibit two breaks in the semilogarithmic plot. The one at lower concentration indicates the point at which the compound starts to accumulate at the interface. It is assigned to $1/K_{aw}$ (air–water partition coefficient), which is a measure of hydrophobicity. The second break is usually attributed to the critical aggregation concentration, CAC, assuming that a formation of aggregates does not cause a further decrease of surface tension. The determined surface properties and related parameters for PBA C8 are the following: $CAC = 3.3 \text{ mM}$, $\gamma_{CAC} = 45 \text{ mN m}^{-1}$, surface excess $\Gamma = 2.55 \mu\text{mol m}^{-2}$, surface area per one molecule at air–water interface $A_s = 65 \text{ \AA}^2$. Properties and efficiency of the PBA C8 as a surfactant can be well compared with properties of above-mentioned structurally similar surfactants: *N*-alkylpyridine-3-boronic¹⁴ acid and 2-oxidodecylpyridine-5-boronic acid.³⁸ Furthermore, to get more information on the structure of the formed nanoparticles in the saturated solution of PBA C8, they were imaged in situ by cryo-TEM microscopy. Cryo-TEM measurements revealed presence of unilamellar vesicles (see Figure S2) of an average diameter 100 nm. This finding is in accordance with results for *N*-alkylpyridine-3-boronic¹⁴ acid and 2-oxidodecylpyridine-5-boronic acid³⁸ where formation of vesicles were observed as well. It is worth mentioning that the *N*-octyl-3-boronopyridinium salt can not reach the CAC within the concentration range of its solubility at 25°C and the formation of vesicles was not observed. This is due to the tendency of *N*-octyl-3-boronopyridinium salt to form a water-deficient bilayer which does not pack into vesicles within studied concentration range.¹⁴ However, the later procedure for mixed PHOS–PEO/PBA nanoparticles preparation involved organic cosolvent and significantly influence self-assembly process that is not comparable with spontaneous vesicles formation in aqueous solution.

Association Behavior of PHOS–PEO and PBA Mixtures in THF/aq. NaOH. Even though PHOS–PEO is a double hydrophilic block copolymer, for kinetic reasons, it is not directly soluble in water and a cosolvent is needed to prepare well-defined PHOS–PEO nanoparticles in aqueous solution.²⁸ As described earlier, only precise tuning of the composition of the mixture of aqueous NaOH with THF in the narrow range between 40 and 50 vol % of THF allows for preparation of stable nanoparticles. All investigated PBA derivatives dissolve directly in THF; however, only the PBA/*i*-Bu system is soluble in 10 mM NaOH solution. PBA C8 and C12 are insoluble in 10 mM NaOH solution at high concentration that is used in this study and form an unstable emulsion in 40 vol % THF in 10 mM NaOH. In order to obtain stable nanoparticles in 10 mM NaOH solution, the solvent composition used for the initial solubilization of PBA and PHOS–PEO mixture was then chosen to be 40 vol % THF in 10 mM NaOH. Not in all cases the PBA could be totally loaded

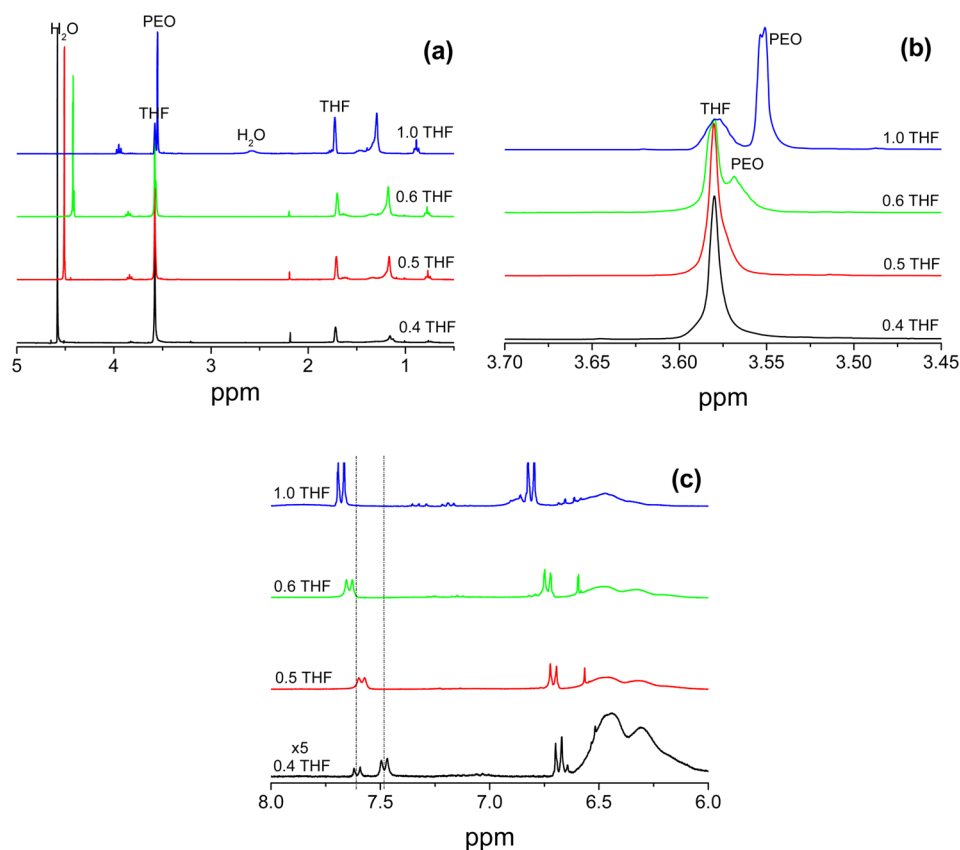


Figure 2. ^1H NMR spectra of PHOS-PEO/C12 solutions in mixtures of THF- d_6 with 10 mM NaOD in D_2O (a), details of the region from 3.45 to 3.70 chemical shift (ppm) (b), and from 6.0 to 8.0 chemical shift (ppm) (c).

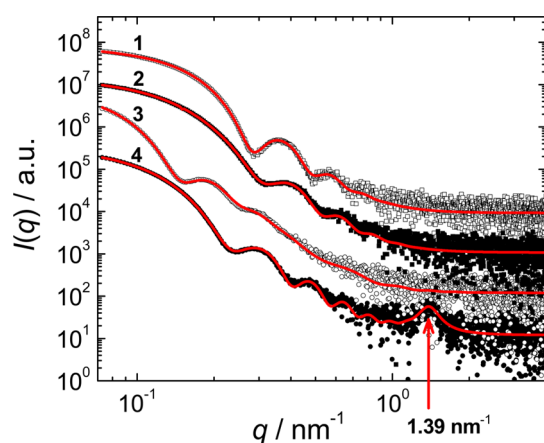


Figure 3. SAXS curves (experimental data and fits) for PHOS-PEO (1), PHOS-PEO/*i*-Bu (2), PHOS-PEO/C8 (3), and PHOS-PEO/C12 (4) coassembled nanoparticles. Intensities of the data are incrementally shifted up by a factor 8 for better readability; data for the PHOS-PEO/C12 are directly at scale.

into the nanoparticles, especially PBA *i*-Bu that is directly soluble in 10 mM NaOH solution and could escape from the semipermeable membrane during removal of the organic solvent from the nanoparticle dispersion by dialysis. However, in the case of insoluble PBA C12 and C8 in 10 mM NaOH, we can assume that most of PBA is encapsulated in the nanoparticles because otherwise we would observe some precipitation during dialysis. Figure 1 shows a typical CONTIN distribution (measured at the scattering angle, $\theta = 90^\circ$) of the

Table 1. Parameters Obtained from Fitting the SAXS Curves for PHOS-PEO/PBA Systems

sample	$R_1 \pm \sigma_1$, nm	$R_2 \pm \sigma_2$, nm	x_2^a
PHOS-PEO/C12 ^b	19 ± 5	19 ± 1	0.363
PHOS-PEO/C8	29 ± 4	9^c	0.001
PHOS-PEO/ <i>i</i> -Bu	16 ± 4	14 ± 1	0.334
PHOS-PEO	15 ± 2^{d}		

^a $x_2 = N_2/(N_1 + N_2)$. ^bScattering peak parameters, $q_c = 1.39 \text{ nm}^{-1}$ and $\sigma_3 = 0.75 \text{ nm}^{-1}$. ^cMonomodal Gaussian distribution. ^dMonodisperse spheres.

apparent hydrodynamic radii of PHOS-PEO/PBA aggregates in THF (40 vol %)/10 mM NaOH mixture. The $R_{\text{H}}^{\text{APP}}$ distributions for PHOS-PEO and PHOS-PEO/C12 consist of two modes corresponding to individual PHOS-PEO chains and large PHOS-PEO and PHOS-PEO/C12 aggregates, respectively. In the case of PHOS-PEO/*i*-Bu and PHOS-PEO/C8, an additional intermediate mode appears, corresponding probably to individual *i*-Bu and C8 aggregates, respectively. The latter hypothesis was tested also by the spin-echo NMR spectroscopy. For a proper understanding and comparison of the values measured by NMR and by dynamic light scattering, it is necessary to keep in mind that NMR yields the number-average data while DLS provides z -averages which are strongly affected by large scatterers.

Chemical shifts in the range from 6.3 to 6.7 ppm corresponding to aromatic protons of PHOS block, which appeared as broad signals, have almost the same diffusion coefficients $1.48 \times 10^{-11} \text{ m}^2\text{s}^{-1}$ as those of aromatic protons

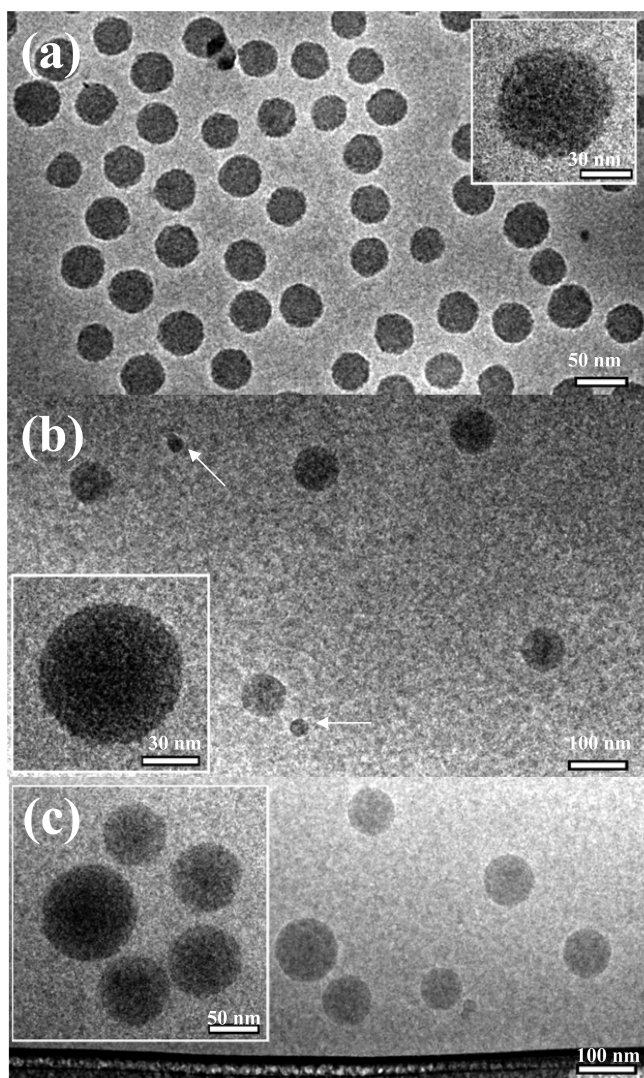


Figure 4. Cryo-TEM images of (a) PHOS-PEO/C12, (b) PHOS-PEO/C8, and (c) PHOS-PEO/*i*-Bu nanoparticles in 10 mM NaOH solution.

~6.8 and ~7.7 ppm corresponding to PBA C12 (1.16×10^{-11} and $1.29 \times 10^{-11} \text{ m}^2 \text{ s}^{-1}$, respectively). It indicates that PBA-PEO and PBA molecules are well intermixed and involved in the formation of one nanoparticle. However, in the case of PHOS-PEO/C8 and PHOS-PEO/*i*-Bu mixtures, the diffusion coefficients of PHOS protons are much influenced by the presence of PBA, that is, 3.28×10^{-12} and $5.8 \times 10^{-12} \text{ m}^2 \text{ s}^{-1}$, respectively and differ significantly from that measured for pure PHOS-PEO, $2.13 \times 10^{-11} \text{ m}^2 \text{ s}^{-1}$. Due to higher solubility of PBA C8 and *i*-Bu in 40% THF solution not all PBA molecules are involved in the association with copolymer allowing to detect diffusion coefficient of individual PBA *i*-Bu molecules that is 2.0×10^{-10} and $2.03 \times 10^{-10} \text{ m}^2 \text{ s}^{-1}$ and some preaggregates of PBA C8 2.60×10^{-11} and $2.87 \times 10^{-11} \text{ m}^2 \text{ s}^{-1}$. The interplay of association and solubility of both components allows to tune precisely structure and properties of the resulting nanoparticles. It is worth mentioning that the particles in the system PHOS-PEO/C8 in 40% THF solution are growing with time. That allows one to quench nanoparticles at different periods of time and introduce another parameter that can be varied in the preparation of desired nanoparticles.

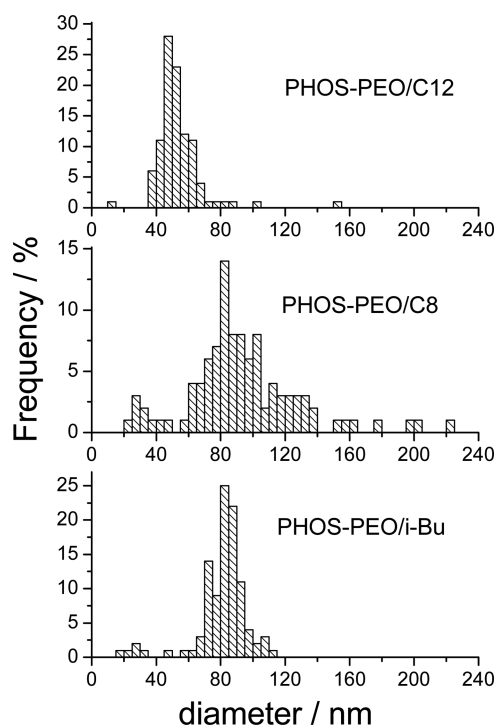


Figure 5. Size distribution functions of PHOS-PEO/PBA nanoparticles as seen by cryo-TEM.

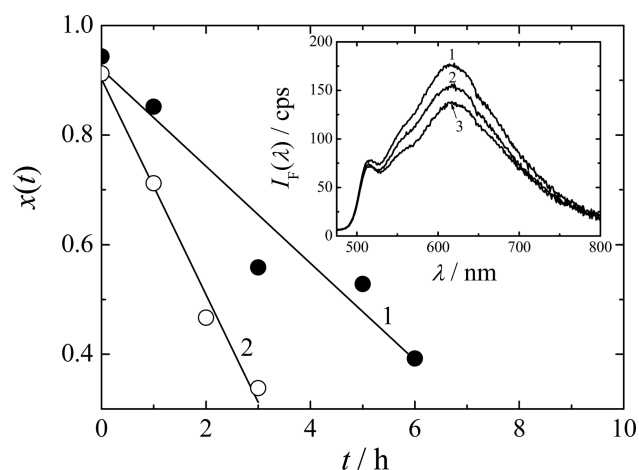


Figure 6. Fractions of particle-embedded ARS emission intensity, $x(t)$, (eq 4) as a function of time in the presence of glucose (2 mg/mL): (1) PHOS-PEO/C12 and (2) PHOS-PEO/C8. Inset: ARS emission spectra ($\lambda_{\text{ex}} = 468 \text{ nm}$) for PHOS-PEO/C12 nanoparticles in ARS immediately (curve 1) and 6 h (curve 2) after addition of glucose and for free ARS in water (curve 3).

Table 2. $R_{\text{H}}^{\text{app}}$ Obtained from the DLS Measurements for PHOS-PEO/PBA Systems and after Glucose Addition

sample	no GLU	1 mg/mL GLU	3 mg/mL GLU	5 mg/mL GLU
$R_{\text{H}}^{\text{app}}_{\text{PHOS-PEO/C12/nm}}$	36	39	46	51
$R_{\text{H}}^{\text{app}}_{\text{PHOS-PEO/C8/nm}}$	48	54	59	67

Figure 2 shows ^1H NMR spectra of PHOS-PEO/C12 in mixtures of THF- d_8 with 10 mM NaOD in D_2O at various mixture compositions from pure THF- d_8 to 40% v/v THF- d_8 . With the increasing content of NaOD_{aq} , the signals of the copolymer and C12 broaden and decrease as a result of both

hindered mobility of the system and due to the association of copolymer chains with C12. The interaction of –OH groups of the PHOS block and –B(OH)₂ groups involved formation of the anionic group –B(OH)₃[–] that still attracts –CH₂O– groups of PEO to form hydrogen bonds. The PEO block is more likely interacting with anionic species such as sodium dodecyl sulfate,⁴⁰ than with cationic ones. It is noteworthy that the interaction of C12 with PHOS–PEO most probably involves, formation of the ester bond between hydroxyl groups of PHOS block and boronic acid groups of PBA C12, which is evident from the presence of additional signal at about 7.6 ppm in solution containing the highest content on NaOD_{aq} (Figure 2c). This phenomenon was observed only for the PHOS–PEO/PBA C12 system, indicating that to detect the esterification reaction by NMR within nanoparticles the spatial proximity of the reacting groups is needed, however we do not preclude formation of ester bonds in the case of PHOS–PEO/PBA C8 and PHOS–PEO/PBA *i*-Bu systems. Wooley et al. demonstrated that photoactive multicompartiment nanostructures (MCNs) can be formed using photophysically active pyrazine-based diamino cross-linkers of different spacer length.⁴¹ The cross-linking not only enhances the stability of MCMs to afford MCNs with hydrophilic shells but also allows for tuning of the MCN internal spacing, through varying the chemical structures and the incorporation stoichiometry of the cross-linkers. These MCNs exhibit unique fluorescence emission characteristics, upon exposure to external environments at different pH values. However, authors was not able to prove amidation reaction between cross-linker and block copolymer within nanoparticles by NMR or IR techniques.

ζ-Potential Measurements. Electrophoretic light scattering measurements showed that the ζ-potential of the PHOS–PEO/PBA nanoparticles changed from –40 mV at pH 12 to –14 mV at pH 9 (see Figure S3, ζ-potential of PHOS–PEO and PHOS–PEO/PBA nanoparticles as a function of pH). This indicates that the nanoparticles are stabilized by the negative charge of the PHOS–PEO/PBA complex located within a surface region. Similarly to the previously studied PHOS–PEO nanoparticles,²⁸ titration with hydrochloric acid causes instability and precipitation of PHOS–PEO/PBA nanoparticles at pH < 9 due to protonation of –O[–] groups of PHOS and/or –B(OH)₃[–] groups of PBA and increasing of ionic strength. However, when doing dialysis to pure water it is possible to lower solution pH closer to physiological one (pH ca. 7.5) while the nanoparticles retain their negative surface charge at high enough values to keep them electrostatically stabilized. It is possible that adsorption of OH[–] on the nanoparticles contributes to the negative surface charge

SAXS Studies of Hybrid Nanoparticles. In order to obtain information about the size and structure of coassembled nanoparticles formed by the PHOS–PEO copolymer and the PHOS–PEO/PBA mixed systems, we performed small-angle X-ray scattering experiments.

Scattering curves (Figure 3) were fitted by the model in which the nanoparticles are treated as noninteracting homogeneous polydisperse spheres,

$$I_{\text{sphere}}(q) = 16\pi^2(\Delta\eta)^2 \int_0^\infty \sum_{i=1}^2 N_i G(R, R_i, \sigma_i) \times \left[\frac{\sin(qR) - qR\cos(qR)}{q^3 R^3} \right]^2 R^6 dR \quad (1)$$

where $\Delta\eta$ is the excess scattering length density of the spheres and N_1, N_2 are the number concentrations of the two populations of the spheres with the Gaussian distribution $G(R, R_i, \sigma_i)$ of the sphere radius R ,

$$G(R, R_i, \sigma_i) = \left\{ \sqrt{\frac{\pi}{2}} \sigma_i \left[1 + \operatorname{erf}\left(\frac{R_i}{\sqrt{2}\sigma_i}\right) \right] \right\}^{-1} \times \exp\left[-\frac{(R - R_i)^2}{2\sigma_i^2}\right] \quad (2)$$

where R_i, σ_i , respectively, are the center and the full width in half-maximum (fwhm) of the distribution. The values of the fits are summarized in Table 1.

In the case of the PHOS–PEO/C12 complex, a weak structure peak appears in the high q region which reflects close packing of the C12 micelles in the formed nanoparticles. (The presence of similar structure peaks was reported for several systems containing double hydrophilic block polyelectrolytes (DPBP) and oppositely charged surfactants, both in the bulk⁴² and in the cores of DHBP core–shell nanoparticles.^{43–45}) In the model used, the structure peak was described as an additional contribution to the scattering function expressed by the structure factor for disordered cell–cell correlations,⁴⁶

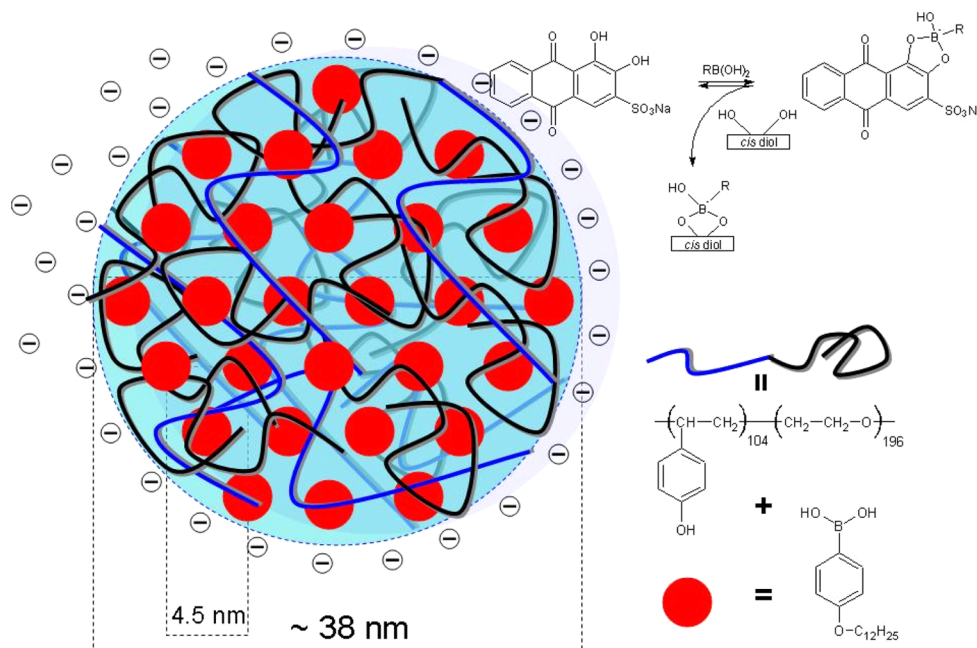
$$I_{\text{peak}}(q) = \frac{I_0 \xi^{-2}}{(q - 2\pi l^{-1})^2 + \xi^{-2}} \quad (3)$$

where l is the characteristic packing distance and ξ is the correlation length. The fit provides values, $l = 4.52$ nm and $\xi = 1.3$ nm.

Cryogenic Transmission Electron Microscopy. In order to confirm the model used for the treatment of the SAXS data, PHOS–PEO/PBA nanoparticles were visualized in situ by cryo-TEM. All micrographs in Figure 4 show individual spherical particles with different size distributions. The average radii of the nanoparticles observed on the micrographs are 27 ± 7 nm for PHOS–PEO/C12, 47 ± 18 nm for PHOS–PEO/C8, and 41 ± 8 nm for PHOS–PEO/*i*-Bu. This finding is in reasonable agreement with the data obtained from the SAXS measurements. It is worth mentioning that the size distribution function Figure 5 (at least hundred of nanoparticles were taken under consideration to construct distribution profiles) for PHOS–PEO/C8 shows bimodal size distribution (small nanoparticles are indicated by arrows in Figure 4b; see also Supporting Information Figure S4); this is in accordance with the results obtained from SAXS measurements. The slight differences in sizes obtained from cryo-TEM and LS could be attributed to the fact that the cryo-TEM results are number-averaged, while the DLS results are based on z -averaged diffusion coefficients.⁴⁷ It is interesting to mention that pure PHOS–PEO nanoparticles (see Figure S5) are slightly larger than that of PHOS–PEO/PBA systems with average radii of 60 nm, resembling rather a core–shell structure than homogeneous spheres. This difference can be explained based on previous discussion on slow solubilization of PHOS block. The pure PHOS–PEO nanoparticles were investigated by cryo-TEM 1.5 years after their preparation which is the sufficient length scale for the change in the association number and size of the particles.

Fluorescence Study of Glucose-Triggered Release of Alizarin Red S from PHOS–PEO/PBA Nanoparticles. Competitive binding of 1,2- or 1,3-diols to PBA can in

Scheme 3. Schematic Drawing of the Coassembled Structure in Solution of PHOS–PEO/C12 As Seen by SAXS and Competitive Binding of Boronic Acid with Alizarin Red S and *cis*-Diol



principle be used both for loading such compounds into PHOS–PEO/PBA nanoparticles as well as for their triggered release by adding another 1,2- or 1,3-diol to the nanoparticles solution. In order to study such loading and triggered release, we chose Alizarin Red S (ARS) as a model compound with a 1,2-dihydroxy bond and glucose as an agent triggering the ARS release from PHOS–PEO/PBA nanoparticles. Since the ARS fluorescence quantum yield in the aqueous solution is lower than that in PHOS–PEO/PBA nanoparticles, the loading and release of ARS can be followed by fluorescence measurements.

Assuming that all ARS in the PHOS–PEO (1 mg/mL)/PBA (2.5 mM) aqueous solution is bound to PBA in the nanoparticles prior to the addition of glucose, and that the increase of the sample volume due to the addition of the stock solution of glucose can be neglected, we can calculate the fraction of ARS embedded in PHOS–PEO/PBA nanoparticles at the time t after the addition of glucose, $x(t)$, as

$$x(t) = \frac{I(t) - I_w}{I_{np} - I_w} \quad (4)$$

where $I(t)$ is the emission intensity from the solution at the time t after the addition of glucose, I_{np} is the emission intensity from the solution before the addition of glucose, and I_w is the emission intensity of aqueous solution of 0.1 mM ARS (the same concentration as in PHOS–PEO/PBA aqueous solutions).

The results are shown in Figure 6. The integral intensities over the emission band of ARS from 480 to 800 nm upon excitation at 468 nm (inset of Figure 6) were taken for the calculation of $x(t)$ values. The $x(t)$ fraction slightly drops after the addition of glucose, probably due to the triggered fast release of ARS bound at the surface or close to the surface of the nanoparticles. This fast release regime is followed by the slower one on the time scale of hours, controlled by the transport of glucose and the probe to and from the nanoparticle interior. Since the more hydrophilic PHOS–PEO/C8 nano-

particles allow for a faster exchange of glucose and ARS (which are both hydrophilic), the ARS release and the consequent fluorescence emission decrease is faster for PHOS–PEO/C8 than for PHOS–PEO/C12.

The response of PHOS–PEO/PBA assemblies on glucose in 10 mM NaOH was monitored by dynamic light scattering. After addition of an appropriate amount of glucose to nanoparticles, samples were left for 24 h to equilibrate and ensure full reaction between glucose and phenylboronic acid groups. Both PHOS–PEO/C8 and PHOS–PEO/C12 nanoparticles swell upon addition of glucose as indicated by the increase of hydrodynamic radius, R_H , as shown in Table 2.

CONCLUSION

In this paper, we show that novel well-defined compact spherical nanoassemblies of double hydrophilic block copolymer poly(4-hydroxystyrene)-*block*-poly(ethylene oxide) and phenylboronic acids of different hydrophobicity can be prepared by subsequent dialysis of PHOS–PEO/PBS solutions in THF/aq.NaOH mixtures against aqueous buffers. The SAXS investigation revealed that only mixture of PBA C12 and PHOS–PEO self-assemble into spherical nanoobjects with unique morphology (Scheme 3) consisting of closely packed C12 micelles embedded in intermixed PHOS–PEO nanoparticles. Spatial proximity of PHOS–PEO and PBA C12 induced formation of ester bonds that is already seen in the mixture of NaOH_{aq}/THF by ¹H NMR. Due to the presence of PBA moieties within the nanoparticles, the species are able to covalently bind ARS as a model diol. The latter feature has been confirmed by fluorescence measurements within the competition assay with glucose, that is tunable by changing hydrophobicity of the PBA. Nanoparticles were proved to exhibit swelling in response to glucose as monitored by light scattering. Thus, this new type of nanoparticles is a promising platform as a glucose-responsive drug delivery vehicles.

■ ASSOCIATED CONTENT

■ Supporting Information

The Supporting Information is available free of charge on the ACS Publications website at DOI: 10.1021/acs.biomac.5b01325.

It contains additional cryo-TEM images, pH dependence of ξ -potential and surface tension (PDF).

■ AUTHOR INFORMATION

Corresponding Author

*E-mail: uchman@natur.cuni.cz. Fax: +420 22499752. Tel: +420 221951292.

Notes

The authors declare no competing financial interest.

■ ACKNOWLEDGMENTS

The authors acknowledge the financial support from the Ministry of Education, Youth and Sport of the Czech Republic (7AMB13PL025), Czech Science Foundation Grant P205/14-14608S (M.U.), and Polish Ministry of Science and Higher Education (8771/R13/R14) as well as the support of Faculty of Chemistry, Warsaw University of Technology. L.K. acknowledges the support of the grant P302/12/G157 from the Czech Science Foundation, Prvrouk/1LF/1 and UNCE204022 from the Charles University in Prague. This work has been supported by the European Union in the framework of European Social Fund through the Warsaw University of Technology Development Programme, by the scholarship awarded by the Center of Advanced Studies for A.M. for 6 months stay at Charles University in Prague under supervision of M. U.

■ REFERENCES

- (1) The Lancet. The diabetes pandemic. *Lancet* **2011**, *378*, 99.
- (2) Li, M. G.; Lu, W. L.; Wang, J. C.; Zhang, X.; Wang, X. Q.; Zheng, A. P.; Zhang, Q. *Int. J. Pharm.* **2007**, *329*, 182–191.
- (3) Harada, A.; Kataoka, K. *Prog. Polym. Sci.* **2006**, *31*, 949–982.
- (4) Liu, G.; Ma, R.; Ren, J.; Li, Z.; Zhang, H.; Zhang, Z.; An, Y.; Shi, L. *Soft Matter* **2013**, *9*, 1636–1644.
- (5) Yao, Y.; Wang, X.; Tan, T.; Yang, J. *Soft Matter* **2011**, *7*, 7948–7951.
- (6) Wang, B.; Ma, R.; Liu, G.; Li, Y.; Liu, X.; An, Y.; Shi, L. *Langmuir* **2009**, *25*, 12522–12528.
- (7) Adamczyk-Woźniak, A.; Czerwińska, K.; Madura, I. D.; Matuszewska, A.; Sporyński, A.; Żubrowska-Zembrzaska, A. *New J. Chem.* **2015**, *39*, 4308–4315.
- (8) Kuivila, H. G.; Keough, A. H.; Soboczanski, E. J. *J. Org. Chem.* **1954**, *19*, 780–783.
- (9) Springsteen, G.; Wang, B. *Chem. Commun.* **2001**, 1608–1609.
- (10) Adamczyk-Woźniak, A.; Borys, K. M.; Madura, I. D.; Pawelko, A.; Tomecka, E.; Żukowski, K. *New J. Chem.* **2013**, *37*, 188–194.
- (11) Yang, W.; Gao, X.; Wang, B. *Med. Res. Rev.* **2003**, *23*, 346–368.
- (12) Korček, S.; Watts, G. B.; Ingold, K. U. *J. Chem. Soc., Perkin Trans. 2* **1972**, 242–248.
- (13) Savsunenko, O.; Matondo, H.; Karpichev, Y.; Poinot, V.; Popov, A.; Rico-Lattes, I.; Lattes, A. *J. Surfactants Deterg.* **2012**, *15*, 345–350.
- (14) Savsunenko, O.; Matondo, H.; Franceschi-Messant, S.; Perez, E.; Popov, A. F.; Rico-Lattes, I.; Lattes, A.; Karpichev, Y. *Langmuir* **2013**, *29*, 3207–3213.
- (15) Springsteen, G.; Wang, B. *Tetrahedron* **2002**, *58*, 5291–5300.
- (16) Kataoka, K.; Miyazaki, H.; Bunya, M.; Okano, T.; Sakurai, Y. *J. Am. Chem. Soc.* **1998**, *120*, 12694–12695.

- (17) Matsumoto, A.; Ishii, T.; Nishida, J.; Matsumoto, H.; Kataoka, K.; Miyahara, Y. *Angew. Chem., Int. Ed.* **2012**, *51*, 2124–2128.
- (18) Hoare, T.; Pelton, R. *Macromolecules* **2007**, *40*, 670–678.
- (19) Ancla, C.; Lapeyre, V.; Gosse, I.; Catargi, B.; Ravaine, V. *Langmuir* **2011**, *27*, 12693–12701.
- (20) Xing, S.; Guan, Y.; Zhang, Y. *Macromolecules* **2011**, *44*, 4479–4486.
- (21) Liu, P.; Luo, Q.; Guan, Y.; Zhang, Y. *Polymer* **2010**, *51*, 2668–2675.
- (22) Roy, D.; Cambre, J. N.; Sumerlin, B. S. *Chem. Commun.* **2009**, 2106–2108.
- (23) Wang, Y.; Zhang, X.; Han, Y.; Cheng, C.; Li, C. *Carbohydr. Polym.* **2012**, *89*, 124–131.
- (24) Yang, H.; Sun, X.; Liu, G.; Ma, R.; Li, Z.; An, Y.; Shi, L. *Soft Matter* **2013**, *9*, 8589–8599.
- (25) Ma, R.; Yang, H.; Li, Z.; Liu, G.; Sun, X.; Liu, X.; An, Y.; Shi, L. *Biomacromolecules* **2012**, *13*, 3409–3417.
- (26) Yao, Y.; Zhao, L.; Yang, J.; Yang, J. *Biomacromolecules* **2012**, *13*, 1837–1844.
- (27) Mountrichas, G.; Pispas, S. *J. Polym. Sci., Part A: Polym. Chem.* **2007**, *45*, 5790–5799.
- (28) Stepanek, M.; Hajduova, J.; Prochazka, K.; Slouf, M.; Nebesarova, J.; Mountrichas, G.; Mantzaridis, C.; Pispas, S. *Langmuir* **2012**, *28*, 307–313.
- (29) Pinto, M. S.; McGahan, M. E.; Steiner, W. W.; Priefer, R. *Colloids Surf, A* **2011**, *377*, 182–186.
- (30) Barclay, G. G.; Hawker, C. J.; Ito, H.; Orellana, A.; Malenfant, P. R. L.; Sinta, R. F. *Macromolecules* **1998**, *31*, 1024–1031.
- (31) Martini, F.; Borsacchi, S.; Geppi, M.; Pilati, F.; Toselli, M. *Polymer* **2011**, *52*, 4536–4544.
- (32) Jańczyk, M.; Adamczyk-Woźniak, A.; Sporyński, A.; Wróblewski, W. *Anal. Chim. Acta* **2012**, *733*, 71–77.
- (33) Soundararajan, S.; Badawi, M.; Kohlrust, C. M.; Hageman, J. H. *Anal. Biochem.* **1989**, *178*, 125–134.
- (34) Jerschow, A.; Muller, N. *J. Magn. Reson.* **1997**, *125*, 372.
- (35) Johnson, C. S. *Prog. Nucl. Magn. Reson. Spectrosc.* **1999**, *34*, 203.
- (36) Longworth, L. G. *J. Phys. Chem.* **1960**, *64*, 1914.
- (37) Dubochet, J.; Adrian, M.; Chang, J. J.; Homo, J. C.; Lepault, J.; McDowell, A. W.; Schultz, P. Q. *Q. Rev. Biophys.* **1988**, *21*, 129.
- (38) Maiti, M.; Roy, A.; Roy, S. *Langmuir* **2013**, *29*, 13329.
- (39) Hall, D. G. *Boronic Acids. Preparation and Applications in Organic Synthesis, Medicine and Materials*, Second ed., Completely Revised Edition; Hall, D. G., Ed.; Wiley-VCH: Weinheim, 2011; p 10.
- (40) Barbosa, A. M.; Santos, I. J. B.; Ferreira, G. M. D.; da Silva, M. D. H.; Teixeira, A. V. N. D.; da Silva, L. H. M. *J. Phys. Chem. B* **2010**, *114*, 11967–11974.
- (41) Sun, G.; Cui, H.; Lin, L. Y.; Lee, N. S.; Yang, Ch.; Neumann, W. L.; Freskos, J. N.; Shieh, J. J.; Dorshow, R. B.; Wooley, K. L. *J. Am. Chem. Soc.* **2011**, *133*, 8534–8543.
- (42) Hanski, S.; Houbenov, N.; Ruokolainen, J.; Chondronicola, D.; Iatrou, H.; Hadjichristidis, N.; Ikkala, O. *Biomacromolecules* **2006**, *7*, 3379–3384.
- (43) Uchman, M.; Štěpánek, M.; Prevost, S.; Angelov, B.; Bednar, J.; Appavou, M.-S.; Gradzielski, M.; Procházka, K. *Macromolecules* **2012**, *45*, 6471–6480.
- (44) Uchman, M.; Gradzielski, M.; Angelov, B.; Tošner, Z.; Oh, J.; Chang, T.; Štěpánek, M.; Procházka, K. *Macromolecules* **2013**, *46*, 2172–2181.
- (45) Uchman, M.; Pispas, S.; Kováčik, L.; Štěpánek, M. *Macromolecules* **2014**, *47*, 7081–7090.
- (46) Lei, N.; Safinya, C. R.; Roux, D.; Liang, K. S. *Phys. Rev. E: Stat. Phys., Plasmas, Fluids, Relat. Interdiscip. Top.* **1997**, *56*, 608–613.
- (47) Shen, S.; Eisenberg, A. *J. Phys. Chem. B* **1999**, *103*, 9473.